

Wigner Crystalline Edges in $\nu \lesssim 1$ Quantum Dots

Eyal Goldmann
Scot R. Renn

Department of Physics, University of California at San Diego, La Jolla, CA 92093
(April 20, 2018)

We investigate the edge reconstruction phenomenon believed to occur in quantum dots in the quantum Hall regime when the filling fraction is $\nu \lesssim 1$. Our approach involves the examination of large dots (≤ 40 electrons) using a partial diagonalization technique in which the occupancies of the deep interior orbitals are frozen. To interpret the results of this calculation, we evaluate the overlap between the diagonalized ground state and a set of trial wavefunctions which we call projected necklace (PN) states. A PN state is simply the angular momentum projection of a maximum density droplet surrounded by a ring of localized electrons. Our calculations reveal that PN states have up to 99% overlap with the diagonalized ground states, and are lower in energy than the states identified in Chamon and Wen's study of the edge reconstruction.

PACS numbers: 71.10.-w, 73.23.Hk, 73.40.Hm, 73.61.-r

I. INTRODUCTION

A number of recent experiments have studied the behavior of a small number N ($1 \sim 100$) of electrons which have been confined to two-dimensional quantum dots. When these quantum dots are subjected to large perpendicular magnetic fields, a rich phenomenology may be observed, much of it due to the same physics underlying the bulk quantum Hall effect [1,2]. In particular, there has been a great deal of interest in the maximum density droplet (MDD) [3–16], which is the small N analog of the bulk $\nu = 1$ state. Experimentally, the MDD has been identified in several studies, including those of Ashoori et al. [3], Klein et al. [4,5], and Oosterkamp et al [6]. Because the MDD's size decreases monotonically with magnetic field, it is clear from electrostatic considerations that a sufficiently strong magnetic field must destabilize the MDD into a lower density state. A number of theoretical studies have discussed a type of instability called an edge reconstruction, in which the decrease in charge density first occurs along a ring just within the MDD's perimeter. In this article we demonstrate that, neglecting the possibility of spin texturing [7–9], the MDD destabilizes into a state in which the droplet edge is best described as a one-dimensional Wigner crystal. The edge reconstructed density profile may then be understood as an angular momentum projection of the crystallized edge.

In an early study of spin-polarized edge reconstructions, Chamon and Wen [10] identified approximate ground states of the quantum dot by minimizing its energy over single Slater determinants of symmetric gauge lowest Landau level states. They found that increasing the magnetic field forces a transition in which several electrons simultaneously move from *adjacent* states in the interior of the droplet to states at the edge. This state, hereafter referred to as the compact ring (CR) state, therefore consists of a $\nu = 1$ central disk surrounded by

a ring in which all single particle states are completely occupied.

Other studies on smaller dots have revealed a rather different structure. For example, Maksym has studied the electron-electron correlation functions of small droplets ($N \leq 6$) using exact diagonalization [17]. His work finds that for $\nu \ll 1$, the electrons occupy distinct, localized positions relative to each other in a structure which resembles a small piece of a Wigner crystal [18]. In a study of somewhat larger dots, ($N \leq 20$), Muller and Koonin [11] found that for $\nu \lesssim 1$, an approximate Hartree-Fock (HF) Hamiltonian is minimized by a state whose density profile consists of a $\nu \lesssim 1$ central droplet surrounded by a ring of localized electrons.

Given that small dots are expected to Wigner crystallize at high magnetic fields, it seems reasonable to expect that similar behavior would occur in larger dots. However, the crystallization of large dots would differ from that of small dots in at least one important respect: it would occur nonuniformly. This is most evident if one considers a droplet which begins as an MDD, and then evolves into a crystallized state as the magnetic field increases. In this case, any portion of the dot which crystallizes must be partially depopulated, and the extra charge moved to orbitals beyond the MDD perimeter. Since this transfer of charge costs less confinement energy for electrons which begin near the droplet edge, we expect the droplet edge to crystallize first, while the droplet center initially remains liquid [19].

In the following discussion, we will present numerical evidence that the MDD does, in fact, destabilize into an edge crystallized state when the magnetic field increases. To be precise, we will present a partial diagonalization of the many body Hamiltonian with the deep interior orbitals frozen. We will then calculate the overlap of this ground state with the “projected necklace” (PN), a trial wavefunction which exhibits edge crystallization. See Fig. (2). As a result, we find that PN states have

high overlap with diagonalized ground states, and have lower energy than Chamon and Wen's compact ring (CR) state. In addition, we have found that a reconstruction to a PN state may exhibit a much weaker addition spectrum signature than does a reconstruction to a CR state. Whether the reconstruction signature is, in fact, weak depends on the detailed form of the confinement potential.

II. PROJECTED WIGNER NECKLACE STATES

We begin our study by considering parabolically confined two-dimensional electrons in the presence of a perpendicular magnetic field. The noninteracting Hamiltonian for this problem is

$$H_0 = \frac{1}{2m^*}(\mathbf{p} + \frac{e}{c}\mathbf{A})^2 + \frac{1}{2}m^*\omega_0^2 r^2, \quad (1)$$

where m^* is the band mass, ω_0 is the confinement strength (typically $\hbar\omega_0 \sim 1\text{--}3$ meV), and $\mathbf{A} = \frac{B}{2}(\hat{\mathbf{z}} \times \mathbf{r})$. For sufficiently high B , the only appreciably occupied eigenstates of H_0 are the wavefunctions of the lowest Fock-Darwin level (LFDL) [1],

$$\psi_l(\mathbf{r}) = (2^{l+1}\pi l!)^{-1/2} \left(\frac{z}{l_0}\right)^l e^{-|z|^2/4l_0^2}, \quad (2)$$

where l is the angular momentum, $z = x - iy$, and l_0 is the characteristic length, given by $l_0 = l_m \kappa^{-1}$, with $l_m = (\frac{\hbar c}{eB})^{1/2}$, $\kappa = (1 + 4\frac{\omega_0^2}{\omega_c^2})^{1/4}$, and $\omega_c = \frac{eB}{m^*c}$. The angular momentum of ψ_l is l , and its energy is

$$\epsilon_l = \frac{1}{2}\hbar\omega_c (\kappa^2(l+1) - l). \quad (3)$$

Using the ψ_l 's as our basis states, we introduce the second-quantized Hamiltonian for many-electron quantum dots,

$$H = \sum_l \epsilon_l c_l^\dagger c_l + \frac{1}{2} \sum_{ijmn} V_{ijmn} c_i^\dagger c_j^\dagger c_n c_m. \quad (4)$$

Here, V_{ijmn} is the Coulomb interaction [20]

$$V_{ijmn} = \frac{e^2}{\epsilon} \int d^2r_1 d^2r_2 \psi_i^*(\mathbf{r}_1) \psi_j^*(\mathbf{r}_2) \frac{1}{|\mathbf{r}_1 - \mathbf{r}_2|} \psi_m(\mathbf{r}_1) \psi_n(\mathbf{r}_2), \quad (5)$$

and $c_l^\dagger (c_l)$ is the creation (annihilation) operator corresponding to ψ_l .

For the special case of parabolic confinement, the eigenstates of H depend on B only through the l_0 dependence of the single particle orbitals. When B increases, l_0 decreases, and the many-electron states squeeze inward, thereby increasing their Coulomb energy. It follows that, when a quantum dot is subjected to a steadily increasing

magnetic field, its general inward motion will be punctuated by a series of transitions in which the dot jumps to ground states of larger area, and accordingly, larger angular momentum, in order to decrease its Coulomb energy.

The state of lowest total angular momentum L entirely contained in the spin-polarized LFDL is the MDD [10,12], which is simply a single Slater determinant of the N LFDL single particle states with angular momenta $0, 1, \dots, N-1$. Consequently, when N is small, the MDD is the first state in the spin-polarized LFDL to become a ground state of the quantum dot as B increases from zero. A further increase in B will compress the MDD, so that it eventually becomes smaller in diameter than the classical electrostatic solution for a parabolically confined 2D droplet, which is a hemisphere [21]. At this point the contrast between the electronic density and the electrostatic solution is most pronounced at the droplet edge: The electronic density slightly inside (outside) the MDD edge is greater (less) than would be expected from the electrostatic solution. Consequently, the initial destabilization of the MDD at high B involves a redistribution of the charge density at the MDD edge, and leaves the $\nu = 1$ center intact [22].

We seek to characterize these instabilities by introducing a set of trial wavefunctions which incorporate the possibility of crystalline correlations at the $\nu = 1$ edge. To begin, we construct a state which consists of a compact central disk of D electrons surrounded by a necklace of $R = N - D$ localized electrons equally spaced along a ring of radius u . Electrons in the central disk are assumed to occupy wavefunctions ψ_l , given by Eq. (2). Ring electrons are assumed to have orbitals

$$\chi_p(\mathbf{r}) = (2\pi)^{-1/2} \exp \left[-\frac{1}{4l_0^2} (|\mathbf{r} - \mathbf{u}_p|^2 - 2i\hat{\mathbf{z}} \cdot \mathbf{r} \times \mathbf{u}_p) \right] \quad (6)$$

where $\mathbf{u}_p = u(\cos \phi_p, \sin \phi_p)$ are the guiding centers, and $\phi_p = \frac{2\pi p}{R}$, with $p = 0, \dots, R-1$. Our many-body wavefunction is thus

$$\langle \mathbf{r}_0, \dots, \mathbf{r}_{N-1} | N, R, u; WN \rangle = \mathcal{A} \left(\prod_{k=0}^{D-1} \psi_k(\mathbf{r}_k) \prod_{l=D}^{N-1} \chi_{l-D}(\mathbf{r}_l) \right) \quad (7)$$

where \mathcal{A} is the antisymmetrization operator. We call this state a "Wigner necklace". The density profile of a Wigner necklace with $N = 40$, $R = 18$, and $u = 10.5l_0$ is plotted in Fig. (1).

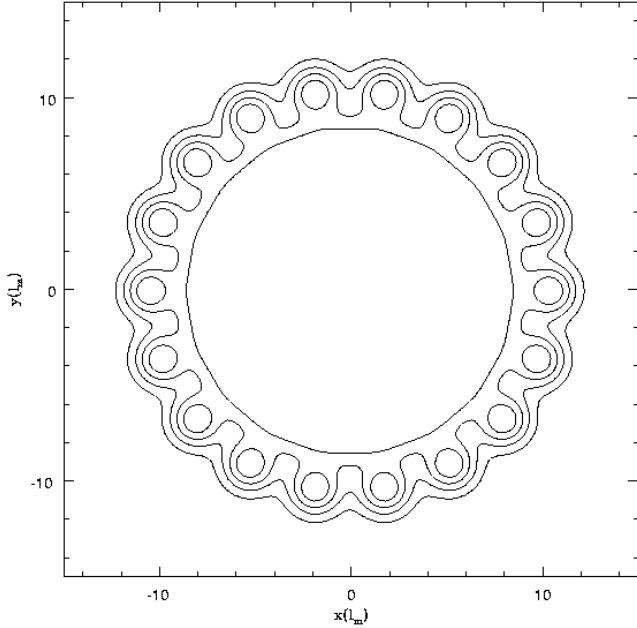


FIG. 1. Density contours of a Wigner necklace state with $N = 40$, $R = 18$, and $u = 10.5l_0$.

In order to project $|N, R, u; WN\rangle$ onto fixed total angular momentum L , we seek to expand it into a sum over Slater determinants of the ψ_l 's. Because only states with a D electron compact central disk contribute to the expansion, it is convenient to define $|D, m_1, \dots, m_R\rangle$ as an N body state consisting of a D electron compact central disk and R additional single particle orbitals, that is,

$$\langle \mathbf{r}_0, \dots, \mathbf{r}_{N-1} | D, m_1, \dots, m_R \rangle = \mathcal{A} \left(\prod_{k=0}^{D-1} \psi_k(\mathbf{r}_k) \prod_{l=D}^{N-1} \psi_{m_{l-D+1}}(\mathbf{r}_l) \right). \quad (8)$$

Defining $P(L)$ to be the operator which projects onto total angular momentum L , we thus have

$$P(L)|N, R, u; WN\rangle = \sum_{m_1 + \dots + m_R = L - \frac{1}{2}D(D-1)} |D, m_1, \dots, m_R\rangle \langle D, m_1, \dots, m_R | N, R, u; WN\rangle, \quad (9)$$

where the sum only includes Slater determinants with the correct total angular momentum. In practice, it is necessary to truncate this sum by disposing of all Slater determinants involving single particle momenta with $m_i > N + k - 1 + W$, where W acts as a cutoff. In this work, we use $W \geq 7$. The coefficients in Eq. (9), which are computed in the Appendix, are given by

$$\langle D, m_1, \dots, m_R | N, R, u; WN \rangle = C \prod_{l=1}^R (m_l!)^{-1/2} \prod_{1 \leq i < j \leq R} \sin\left(\frac{\pi}{R}(m_i - m_j)\right) \quad (10)$$

where C is a constant common to every coefficient in the expansion of a particular $|N, R, u; WN\rangle$.

It follows from (10) (see the Appendix) that if we define $P(L)$ to be the operator which projects states onto total angular momentum L , then $P(L)|N, R, u; WN\rangle = 0$ unless $L = \frac{1}{2}N(N-1) + kR$, where $k = 0, 1, \dots$ (A similar result has been derived in Refs. [17], [23], and [24] for the case of totally crystallized droplets.). Hence, the angular momentum projected states are conveniently defined as

$$|N, R, k; PN\rangle = P\left(\frac{1}{2}N(N-1) + kR\right)|N, R, u; WN\rangle, \quad (11)$$

where PN means “projected necklace.” Note that $|N, R, k; PN\rangle$ is independent of the ring radius u used to construct the unprojected $|N, R, u; WN\rangle$. The $k = 1$ states are particle-hole excitations of the MDD [13].

To illustrate the effect of the angular momentum projection, we examine the electron-electron correlation function

$$P(\mathbf{r}, \mathbf{r}_1) = \langle \Psi^\dagger(\mathbf{r}) \Psi^\dagger(\mathbf{r}_1) \Psi(\mathbf{r}_1) \Psi(\mathbf{r}) \rangle, \quad (12)$$

where $\Psi(\mathbf{r}) = \sum_{l=0}^{\infty} \psi_l(\mathbf{r}) c_l$ [17,25]. In Fig. (2), we plot $P(\mathbf{r}, \mathbf{r}_1)$ for the state $|40, 18, 3; PN\rangle$, where we have fixed $\mathbf{r}_1 = (x, y) = (7.5l_0, 0)$.

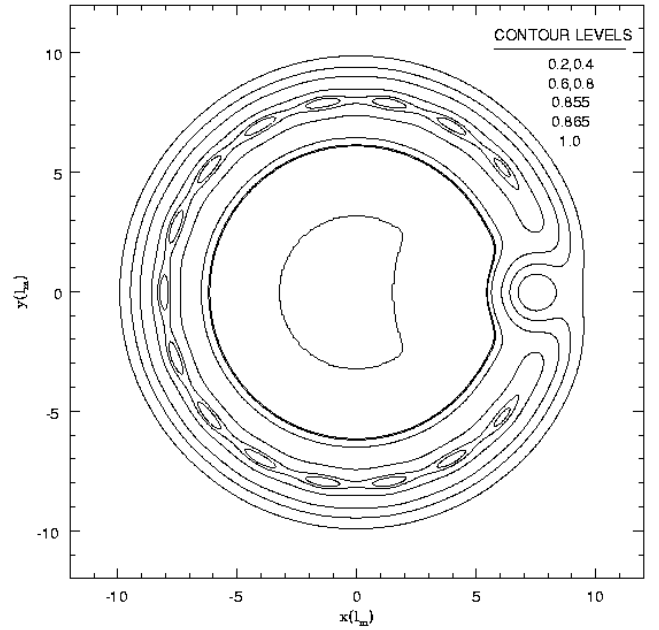


FIG. 2. Two particle correlation function $P(\mathbf{r}, \mathbf{r}_1)$ for the state $|40, 18, 3; PN\rangle$, plotted as a function of \mathbf{r} , with \mathbf{r}_1 fixed at $\mathbf{r}_1 = (7.5l_0, 0)$. $P(\mathbf{r}, \mathbf{r}_1)$ was rescaled so that its maximum value is one. In order to emphasize the state's axial modulation, extra contours were added at levels 0.855 and 0.865.

We note that this state is the lowest energy PN state with $N = 40$ when $\hbar\omega = 1.6\text{meV}$ and $B = 2.42\text{T}$. See Fig. (6) and the accompanying discussion, which will follow. Indeed, a modulation of $P(\mathbf{r}, \mathbf{r}_1)$ is evident at the droplet's edge, but is much weaker than the localization

in the unprojected WN. Extra contours were added to the figure in order to reveal the effect (see the caption).

It is instructive to note the similarities between the PN states and the compact ring (CR) states discussed earlier. Formally, we define the CR state $|N, R, k; CR\rangle$ to be a Slater determinant constructed from the single particle LFDL states with angular momenta $l = 0, \dots, D-1$ and angular momenta $l = D+k, \dots, N+k-1$, where $D = N - R$, as above. Both $|N, R, k; CR\rangle$ and $|N, R, k; PN\rangle$ may be thought of as states formed by moving k electrons from the bulk to the edge of an N electron MDD in order to separate an R electron ring from an $N - R$ electron core. Furthermore, for a given triplet (N, R, k) , $|N, R, k; CR\rangle$ and $|N, R, k; PN\rangle$ have the same total angular momentum L . It follows from Eqs. (3) and (4) that the sum of kinetic and confinement energies of the two states is the same for all B . Therefore, the state with the lower Coulomb energy will be favored for all B .

Motivated by this observation, we have made pairwise comparisons of the Coulomb energies of the states $|N, R, k; CR\rangle$ and $|N, R, k; PN\rangle$ for all (N, R, k) such that $25 \leq N \leq 60$, $2 \leq R \leq 25$, and $1 \leq k \leq 10$. The ranges of R and k have been selected to include all PN and CR states which are likely to become ground states of the quantum dot at magnetic fields slightly beyond the stability range of the MDD. We have confirmed this selection with appropriate minimizations of the droplet energy with respect to PN states, and in separate calculations, with respect to CR states.

For nearly each triplet (N, R, k) within the stated range, we find that $|N, R, k; PN\rangle$ has the lower Coulomb energy, although the difference is small, typically around $0.1\% \sim 0.3\%$. A sample of this comparison is given in Table (1).

(N, R, k)	Compact Ring	Projected Necklace	$E(CR) - E(PN)$
(40,18,1)	124.577	124.487	0.090
(40,18,2)	123.350	123.222	0.128
(40,18,3)	122.123	121.982	0.141
(40,18,4)	120.914	120.771	0.143
(40,18,5)	119.732	119.593	0.139
(40,18,6)	118.585	118.450	0.134
(40,18,7)	117.475	117.345	0.131
(40,18,8)	116.406	116.277	0.129
(40,18,9)	115.377	115.247	0.130
(40,18,10)	114.389	114.260	0.129

TABLE I. Comparison of the Coulomb energies of compact ring states and projected necklace states with $N = 40$, $R = 18$, and $k = 3$. All energies are in units of $\frac{e^2}{\epsilon l_0}$.

The only triplets in the stated range for which the corresponding CR state has the lower Coulomb energy are $(N, 2, 10)$ for $N = 25, \dots, 30$ and $(25, 3, 10)$. However, these exceptions are not a concern because in this range of $N, R \gg 3$ for the ground state, regardless of whether one assumes that the ground states are CR states or PN states. These results are encouraging, as they show that in the vicinity of the edge reconstruction, the ground state of a HF calculation will necessarily be unstable with respect to at least one PN state.

III. DIAGONALIZATION CALCULATIONS

We wish to further test the validity of the PN states by comparing them with the results of diagonalization calculations. Unfortunately, the systems we are studying are too large to accommodate complete diagonalization. Instead, we restrict the basis of our diagonalization calculation to Slater determinants of LFDL states which include a compact central disk of D electrons, defining $|N, R, k; GS\rangle$ to be the lowest energy eigenstate of H within this basis for which $L = L_{MDD} + kR$, where $L_{MDD} = \frac{1}{2}N(N-1)$. This restriction is reasonable because, as discussed above, ground states with $L \gtrsim L_{MDD}$ are expected to retain a $\nu \approx 1$ center.

In Fig. (3), we display the single particle occupancies of the states $|40, 18, 3, PN\rangle$, $|40, 18, 3, CR\rangle$, and $|40, 18, 3, GS\rangle$.

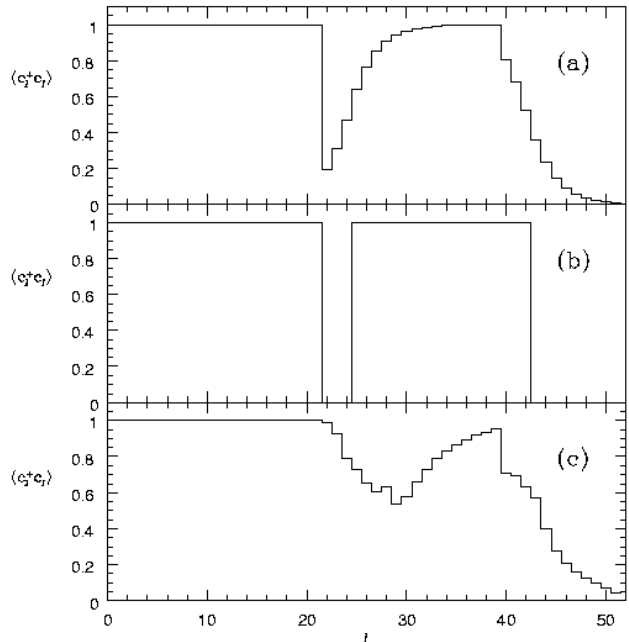


FIG. 3. Panels (a), (b), and (c) show, respectively, the single particle occupancies of the projected necklace state $|40, 18, 3, PN\rangle$, compact ring state $|40, 18, 3, CR\rangle$, and diagonalized state $|40, 18, 3, GS\rangle$.

Clearly, the PN state resembles the diagonalized state

more closely than the CR state does. The main difference between the PN state and the diagonalized state is that the occupancy of the PN state drops sharply at the edge of the central disk. This discrepancy becomes more pronounced as the separation of the ring and central disk increases.

More quantitatively, we have computed $\langle N, R, k; PN | N, R, k; GS \rangle$, the overlap between the diagonalized ground state and the projected necklace state, for states with $N = 30$ and $N = 40$. The results are plotted in Fig. (4).

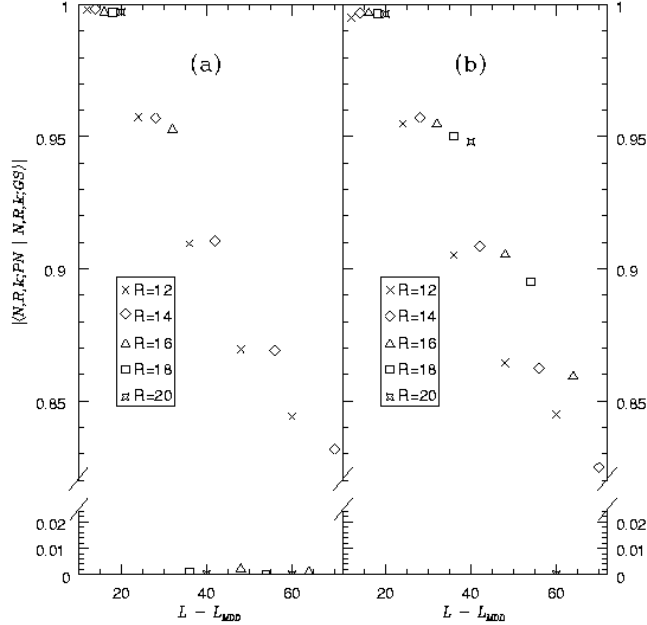


FIG. 4. Overlaps of projected necklace states with ground states of diagonalization calculations. In panels (a) and (b), $N = 30$ and $N = 40$ electrons, respectively. The data in both panels has the pattern of descending staircases, with each step corresponding to a single value of k .

Interestingly, $\langle N, R, k; PN | N, R, k; GS \rangle$ is determined primarily by k . This is evident in Fig. (4), where the data points assemble into a staircase of neat horizontal bunches which descend with increasing k . The numerical values of the overlaps presented range between 0.8–1.0 with the higher overlaps corresponding to smaller k . The $k = 1$ states, whose overlaps consistently exceed 0.99, are particularly successful [13]. On the other hand, $\langle N, R, k; PN | N, R, k; GS \rangle$ often drops to nearly zero (i.e. ≤ 0.002) with increasing k . This effect occurs when some of the ring electrons in the diagonalized ground state become adjoined to the central disk, so that $|N, R, k; GS\rangle$ has, in effect, fewer electrons in its outer ring than $|N, R, k; PN\rangle$. As N increases, the preferred number of electrons in the outer ring increases, and this effect disappears for fixed (R, k) . These results, along with the energetic studies discussed above, demonstrate that the PN states with small k are good approximations

to the edge reconstructed states.

We have also computed $\langle N, R, k; CR | N, R, k; GS \rangle$, the overlap of a compact ring state with the corresponding diagonalized state, for the same triplets (N, R, k) for which we computed $\langle N, R, k; PN | N, R, k; GS \rangle$. The results are plotted in Fig. (5).

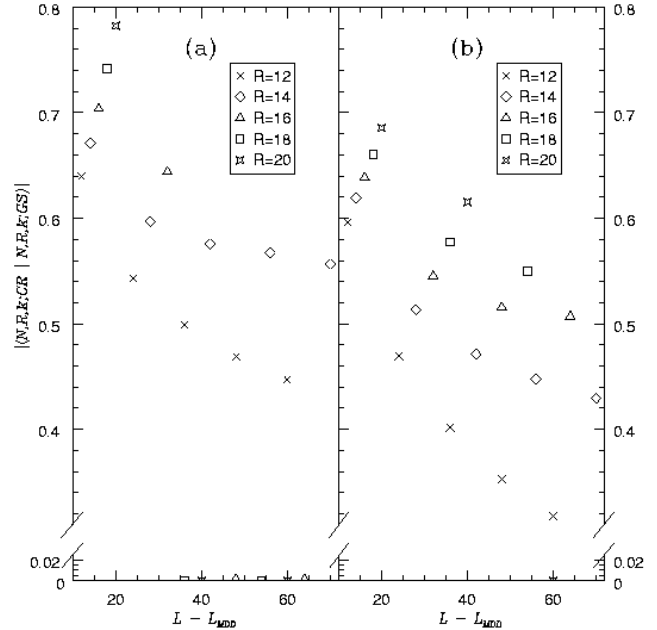


FIG. 5. Overlaps of compact ring (CR) states with ground states of diagonalization calculations. In panels (a) and (b) $N = 30$ and $N = 40$ electrons, respectively. The CR states are less accurate for the larger N , and are consistently less accurate than the projected necklace states.

The computed values of $\langle N, R, k; CR | N, R, k; GS \rangle$ fall in the range 0.3–0.8, except for a few values which are nearly zero (i.e. ≤ 0.002). The set of triplets (N, R, k) for which $\langle N, R, k; CR | N, R, k; GS \rangle$ is nearly zero is exactly the same set of triplets for which $\langle N, R, k; PN | N, R, k; GS \rangle$ is nearly zero. As for the majority of triplets, for which the overlap is substantial (≥ 0.3), $\langle N, R, k; CR | N, R, k; GS \rangle$ is on average 36% less than the corresponding PN overlap when $N = 30$, and 44% less than the corresponding PN overlap when $N = 40$.

IV. ADDITION SPECTRUM CALCULATIONS

We now discuss the consequences of the PN states for an important experimental quantity, the quantum dot addition spectrum. An addition spectrum consists of a sequence of measurements of the chemical potential

$$\mu(N) \equiv E_0(N) - E_0(N - 1), \quad (13)$$

over some range of N , where $E_0(N)$ is the ground state energy of an N -electron quantum dot [3–6]. To perform

this computation, we assume that the ground state in the $\nu \lesssim 1$ regime is the PN state which minimizes the energy, that is, we take

$$E_0(N) = \min_{R,k} \langle N, R, k; PN | H | N, R, k; PN \rangle. \quad (14)$$

The B dependence of $\mu(N)$ for a parabolically confined droplet with $\hbar\omega = 1.6\text{meV}$, as computed from (13) and (14), is plotted in Fig. (6) for $N = 40$ to $N = 46$.

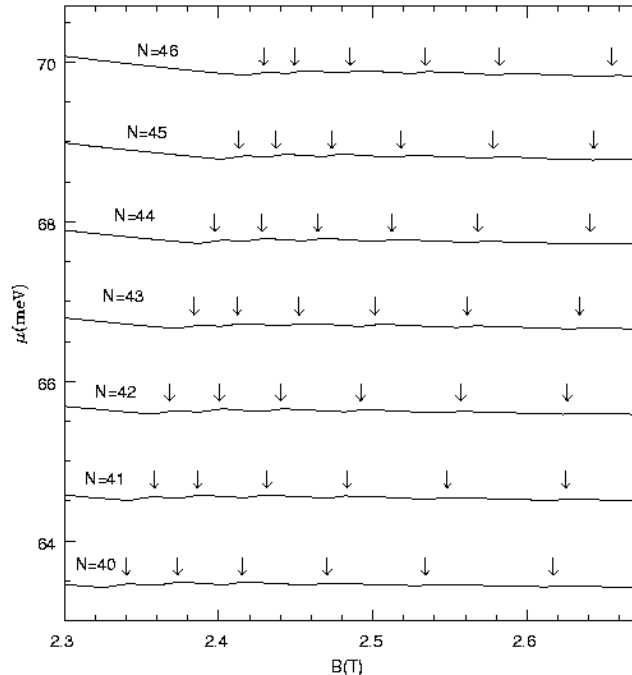


FIG. 6. Addition spectrum traces for a droplet subject to a parabolic confinement of strength $\hbar\omega_0 = 1.6\text{meV}$, computed by energy minimization over projected necklace states. The N th line (as marked) corresponds to the addition of the N th electron into the droplet. Each arrow indicates a unit increase in the N electron droplet's ground state value of k . The leftmost column of arrows denotes the edge reconstruction.

Notably, the addition spectrum traces are nearly featureless in the vicinity of the edge reconstruction, except for small kinks due to increments in k . Recall that k may be understood as the number of holes separating the central disk and the compact edge. As B increases, the ground state value of k for a given N always increases monotonically in unit increments. The first increment of k for a given N , from $k = 0$ to $k = 1$, initiates the edge reconstruction. Each increment in the ground state value of k in the N electron dot is indicated in Fig. (6) by an arrow pointing to the N th addition line. The ground state value of R at the onset of the edge reconstruction is determined mainly by the requirement that the filling fraction at the center of the reconstructed edge be $\nu \lesssim 1$. As N increases from $N = 30$ to $N = 49$, this value increases from $R = 16$ to $R = 20$.

These results are in distinct contrast with the HF result

of Ref. [10], in which the onset of the reconstruction involves the simultaneous transfer of several electrons, and causes a sharp upward jump in the addition spectrum. However, because our approach is based on a more accurate solution of the same Hamiltonian (see preceding discussion), we believe that the cusps seen in Ref. [10] are an artifact of the HF approximation.

On the other hand, experimental work has demonstrated that the high B destabilization of the MDD causes distinct cusps in the addition spectrum of the quantum dot [4,6]. In light of the results presented in Fig. (6), it is thus reasonable to ask whether circumstances exist in which the experimental observation of addition spectrum cusps would even be consistent with spin polarized edge reconstructions.

In fact, we may reintroduce edge reconstruction induced cusps into the addition spectrum by introducing a non-parabolic term into the confinement potential. To be specific, we write $V(r)$ as the sum of the parabolic confinement potential and an additional coffee cup shaped potential, giving

$$V(r) = \frac{1}{2}m^*\omega_0^2r^2 + \beta(r-a)\theta(r-a), \quad (15)$$

where β and a are constants, and $\theta(x)$ is the Heaviside step function. The second quantized many-body Hamiltonian now becomes

$$H = \sum_l (\epsilon_l + \gamma_l) c_l^\dagger c_l + \sum_{ijmn} V_{ijmn} c_i^\dagger c_j^\dagger c_n c_m, \quad (16)$$

with $\gamma_l = \beta \int_a^\infty d^2r \psi_l^*(\mathbf{r})(r-a)\psi_l(\mathbf{r})$.

By exact diagonalization of Eq. (16) within the LFDL, we compute the addition spectra of dots subject to and not subject to a coffee-cup confinement, and plot the results, respectively, in Figs. (7) and (8).

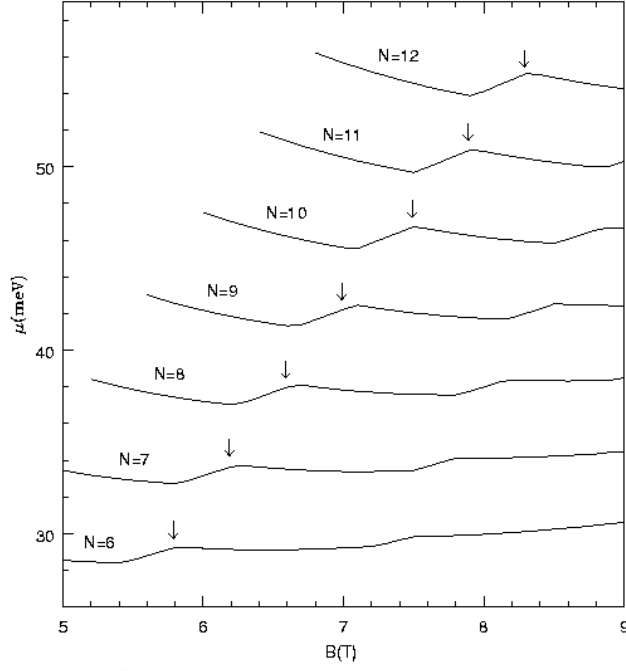


FIG. 7. Addition spectrum traces, computed with exact diagonalization, for a droplet subject to both a parabolic confinement potential of strength $\hbar\omega_0 = 3.0\text{meV}$, and a nonparabolic confinement potential characterized by parameters $a = 40\text{nm}$, and $\beta = 2.0\text{meV/nm}$ (See Eq. (15)). Compare with Fig. 8.

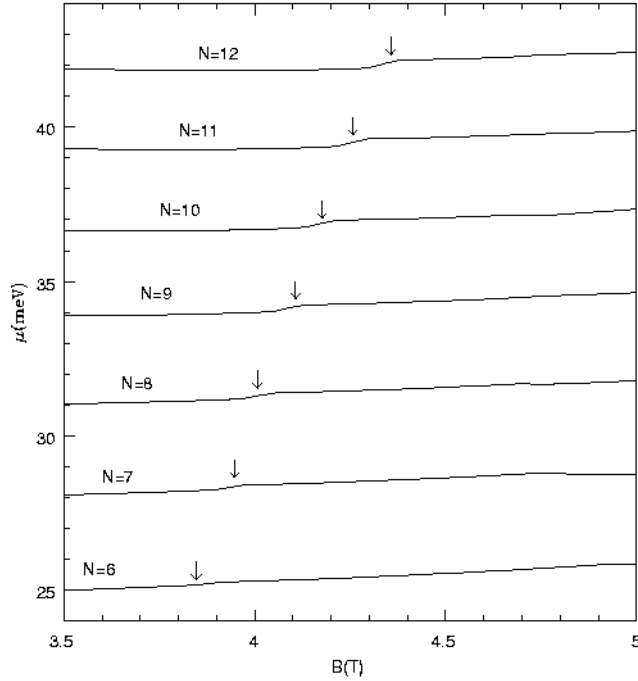


FIG. 8. Addition spectrum traces, computed with exact diagonalization, for a droplet subject to a parabolic confinement of strength $\hbar\omega_0 = 3.0\text{meV}$. Compare with Fig. 7.

For both dots, $\hbar\omega_0 = 3.0\text{meV}$, and for the dot of Fig.

(7), $a = 40\text{nm}$ and $\beta = 2.0\text{meV/nm}$. In these plots, a lone arrow near each addition spectrum trace marks the edge reconstruction. Indeed, the edge reconstruction induced kinks of the nonparabolically confined system are much larger than those of the parabolically confined system. The kink size also increases with electron number, similar to the data of Oosterkamp et al [6].

In summary, we have shown that projected necklace (PN) states accurately describe the spin-polarized instabilities of $\nu \lesssim 1$ quantum Hall droplets. PN states whose total angular momentum differs from that of the MDD by $70\hbar$ or less typically have overlaps with diagonalized states in the range 0.8–0.99. By comparison, the compact ring (CR) states, which are a generalization of the states identified by Chamon and Wen [10], have overlaps of 0.3–0.8 with diagonalized states. We have also shown that near the edge reconstruction, the lowest energy PN state is always lower in energy than the lowest energy CR state. By performing energy minimizations over PN states, we have shown that edge reconstruction induced cusps in the addition spectra of parabolically confined dots are much smaller than suggested by Hartree-Fock [10] studies. Finally, we have shown that large cusps in the addition spectra may occur in dots with nonparabolic confinement potentials.

V. ACKNOWLEDGEMENTS

We would like acknowledge support from the Hellman foundation. We would also like to thank D.P. Arovas, R.C. Ashoori, M.D. Johnson, and J.H. Oaknin for useful conversations and communications.

APPENDIX:

In this appendix, we first compute the coefficient $\langle D, m_1, \dots, m_R | N, R, u; W N \rangle$, introduced in Eq. (9). Recall that in general, the overlap of two Slater determinants $|a_1, \dots, a_K\rangle$ and $|b_1, \dots, b_K\rangle$, where the a_i and b_i are single particle states, is

$$\langle a_1, \dots, a_K | b_1, \dots, b_K \rangle = \begin{vmatrix} \langle a_1 | b_1 \rangle & \dots & \langle a_K | b_1 \rangle \\ \vdots & \ddots & \vdots \\ \langle a_1 | b_K \rangle & \dots & \langle a_K | b_K \rangle \end{vmatrix} \quad (\text{A1})$$

Hence

$$\langle D, m_1, \dots, m_R | N, R, u; W N \rangle = \begin{vmatrix} \mathbf{1}_D & \mathbf{0}_{D \times R} \\ \mathbf{0}_{R \times D} & \mathbf{S}_R \end{vmatrix} \quad (\text{A2})$$

where $\mathbf{1}_D$ is the $D \times D$ unit matrix, due to the inclusion of the D electron compact disk in each state, $\mathbf{0}_{m \times n}$ is the $m \times n$ zero matrix, and

$$\mathbf{S}_R = \begin{pmatrix} \langle \psi_{m_1} | \chi_0 \rangle & \dots & \langle \psi_{m_R} | \chi_0 \rangle \\ \vdots & \ddots & \vdots \\ \langle \psi_{m_1} | \chi_{R-1} \rangle & \dots & \langle \psi_{m_R} | \chi_{R-1} \rangle \end{pmatrix} \quad (\text{A3})$$

To compute \mathbf{S}_R , we use the result $\langle \psi_l | \chi_p \rangle = \alpha_l e^{il\phi_p}$, where $\alpha_l = (2^l l!)^{-1/2} u^l e^{-u^2/4}$. Factoring the α_l 's out of the determinant leaves \mathbf{S}_R in the form of an alternant, which may be readily evaluated, yielding

$$\langle D, m_1, \dots, m_R | N, R, u; WN \rangle = C \prod_{l=1}^R (m_l!)^{-1/2} \prod_{1 \leq i < j \leq R} \sin\left(\frac{\pi}{R}(m_i - m_j)\right), \quad (\text{A4})$$

where C is a constant common to each term in the expansion of a particular $|N, R, u; WN\rangle$. Because of the factor $\prod_{i < j} \sin\left(\frac{\pi}{R}(m_i - m_j)\right)$, $\langle D, m_1, \dots, m_R | N, R, u; WN \rangle$ must vanish if $m_i \equiv m_j \pmod R$ for any pair (m_i, m_j) . This result, along with the observation that there are exactly R m_i 's, lead us to the following lemma:

Lemma 1 For each integer j , $D \leq j \leq D + R - 1$, each state $|D, m_1, \dots, m_R\rangle$ in the expansion of $|N, R, u; WN\rangle$ must include exactly one single particle state ψ_{μ_j} (excluding states in the compact central disk) for which $\mu_j \equiv j \pmod R$. Specifically, we write $\mu_j - j = k_j R$, where k_j is a non-negative integer.

It follows that the total angular momentum of the states in the ring differs from the minimum possible value $\frac{1}{2}R(2D + R - 1)$ by kR , where $k = \sum_{j=D}^{D+R-1} k_j$. The significance of k is discussed in the main body of the text. The lemma is very useful for computation, as it greatly reduces the number of terms in the expansion of a state $|N, R, k; PN\rangle$, and allows us to project wavefunctions $|N, R, u; WN\rangle$ onto values of L which would otherwise be inaccessible.

[1] L. Jacak, P. Hawrylak, and A. Wojs, *Quantum Dots*, (Springer, New York, 1998); T. Chakraborty and P. Pietilainen, *The Quantum Hall Effects*, (Springer-Verlag, New York, 1995).

[2] U. Meirav and E.B. Foxman, *Semicond. Sci. Tech.* **10**, 255 (1995);

[3] R.C. Ashoori, *Nature* **379**, 413 (1996); R.C. Ashoori, H.L. Stormer, J.S. Weiner, L.N. Pfeiffer, K.W. Baldwin, and K.W. West, *Surf. Sci.* **305**, 558 (1994).

[4] O. Klein, C. de C. Chamon, D. Tang, D.M. Abusch-Magder, U. Meirav, X.-G. Wen, M.A. Kastner, and S.J. Wind, *Phys. Rev. Lett.* **74**, 785 (1995).

[5] O. Klein, D. Goldhaber-Gordon, C. de C. Chamon, and M.A. Kastner, *Phys. Rev. B* **53**, R4221 (1996).

[6] T.H. Oosterkamp, J.W. Janssen, L.P. Kouwenhoven, D.G. Austing, T. Honda, and S. Tarucha, *Phys. Rev. Lett.* **82**, 2931 (1999).

[7] J.H. Oaknin, L. Martin-Moreno, C. Tejedor, *Phys. Rev. B* **54**, 16850 (1996).

[8] M.I. Lubin, O. Heinonen, and M.D. Johnson, *Phys. Rev. B* **56**, 10373 (1997).

[9] A. Karlhede and K. Lejnell, *Physica E* **1**, 42, (1997).

[10] C. de C. Chamon and X.G. Wen, *Phys. Rev. B* **49**, 8227 (1994).

[11] H.M. Muller and S.E. Koonin, *Phys. Rev. B* **54**, 14532 (1996).

[12] A.H. MacDonald, S.R.E. Yang, and M.D. Johnson, *Aust. J. Phys.* **46**, 345 (1993).

[13] J.H. Oaknin, L. Martin-Moreno, J.J. Palacios, and C. Tejedor, *Phys. Rev. Lett.* **74**, 5120 (1995). These authors derive a branch of magnetoexcitons equivalent to our $k = 1$ states by postulating that low-lying excitations of the MDD do not involve center of mass motion.

[14] M. Ferconi and G. Vignale, *Phys. Rev. B* **56**, 12108 (1997).

[15] K.H. Ahn, J.H. Oh, and K.J. Chang, *Phys. Rev. B* **52**, 13757 (1995).

[16] S.M. Reimann, M. Koskinen, M. Manninen, and B.R. Mottelson, cond-mat/9904067.

[17] P.A. Maksym, *Phys. Rev. B* **53**, 10871 (1996).

[18] For a review of Wigner crystals in quantum Hall systems, see H.A. Fertig, in *Perspectives in Quantum Hall Effects*, edited by S. das Sarma and A. Pinczuk (Wiley, New York, 1997).

[19] While this manuscript was in preparation, we received a copy of Ref. [16], which makes a similar proposal. Ref. [16] is based on a density functional calculation rather than the diagonalization techniques used here.

[20] We have computed V_{ijmn} using an expansion derived in Michael Stone, H.W. Wyld, and R.L. Schult, *Phys. Rev. B* **45**, 14156 (1992).

[21] V. Shikin, S. Nazin, D. Heitmann, and T. Demel, *Phys. Rev. B* **43**, 11903 (1991).

[22] This has been confirmed by several previous studies, including Refs. [8,10,12,14].

[23] T. Seki, Y. Kuramoto, and T. Nishino, *J. Phys. Soc. Jpn.* **65**, 3945 (1996);

[24] W.Y. Ruan, Y.Y. Liu, C.G. Bao, and Z.Q. Zhang, *Phys. Rev. B* **51**, 7942 (1995).

[25] K. Jauregui, W. Hausler, and B. Kramer, *Europhys. Lett.* **24**, 581 (1993).